Electronic Supplementary Material (ESI) for Journal of Materials Chemistry A.

Electronic Supplementary Information

An intercalation pseudocapacitance-driven perovskite $NaNbO_3$ anode with superior kinetics and stability for advanced lithium-based dual-ion batteries

Tong Yan,[a] Rui Ding,[a]* Danfeng Ying,[a] Yongfa Huang,[a] Yuxi Huang,[a] Caini Tan,[a] Xiujuan Sun,[a]

Ping Gao [a] and Enhui Liu [a]

[a]Key Laboratory of Environmentally Friendly Chemistry and Applications of Ministry of Education, College of Chemistry, Xiangtan University, Xiangtan, Hunan 411105, P.R. China

*E-mails: drm8122@163.com; drm8122@xtu.edu.cn

Table of contents

Experimental section

Synthesis of materials

The chemicals in the experiment were of analytical grade (A.R.) and directly used without further treatment (**Table. S1**). The $NaNbO_3$ sample was synthesized by using a hydrothermal method similar to the literature.[1-3] The compounds of 0.05 M Nb_2O_5 and 0.35 mol NaOH (10 M) were dissolved in 35 mL deionized water, and dispersed well in an ultrasonic bath for 15 min under 100 W power conditions. Secondly, the mixture was transferred into a 50 mL Teflon-lined stainless steel autoclave, which was heated in an electric oven (160 ℃, 18 h), and then cooled down naturally. Next, the yielded precipitates were collected by centrifugal filtration and washed with deionized water several times to neutral, and washed with absolute alcohol at the last time. Finally, the precipitates were dried overnight at 100 ℃ to obtain the products. The synthetic yield of the $NaNbO_3$ of the experiment is about 530 mg (excluding the loss during sample collection), which is 92.3% of the theoretical yield (574 mg).

Characterizations

The phases and crystalline properties were determined by X-ray diffraction (XRD). The surface chemical structures were checked by X-ray photoelectron spectra (XPS). The morphology and size of the particles were analyzed by scanning electron microscopy (SEM) and transmission electron microscopy (TEM). The crystalline microstructures were resolved by high-resolution TEM (HRTEM) and selected area electron diffraction (SAED). The elemental composition and distribution were measured by X-ray energy dispersive spectra (EDS) and mapping.

Electrochemical measurements

The electrodes were prepared by the following two steps: firstly, a well-dispersed mixture of 70 wt% active materials (as-synthesized NNO or commercial graphite KS6), 20 wt% conductive agent (15 wt% acetylene black (AB)+5 wt% superconductive carbon black) and 10 wt% polyvinylidene fluoride binder (PVDF, which was dissolved in N-methyl-2-pyrrolidone (NMP)) were cast onto the current collectors (Cu foil and carbon-coated Al foil were used as the collectors for the anode and cathode respectively, and the thickness was 15 μm), followed by drying in a vacuum oven at 110 ℃ for 12 h; secondly, the electrodes were punched into disks with a diameter of 12 mm, and the mass loading of active materials was about 1.2 mg cm^{-2}. The electrochemical performances were examined by cyclic voltammetry (CV) and galvanostatistic charge-discharge (GCD) tests via CHI660E electrochemical working stations and Neware-CT-4008 testers. Tests for NNO and KS6 electrodes were conducted in half-cells by using the type 2032 coin cells with a certain working electrode (WE), a Li plate as both the counter electrode (CE) and reference electrode (RE), and one piece of glass fiber (GF) as the separator. Tests for NNO//KS6 Li-DIBs s were conducted via full-cells with type 2032 coin cells with equal mass ratio of active materials of NNO anode and KS6 cathode, and the NNO anode was pre-charged (pre-lithiated) at 0.1 A g^{-1} for 4.5 cycles (**Fig. S6**) before the assembly. The electrolytes used in the tests were 1 M $LiPF_6$/EC:EMC:DMC (1:1:1) /1% VC (LBC-305-01, CAPCHEM). All cell assemblies were performed in a high pure Ar-filled dry glove box (MIKROUNA, O_2 and H_2O < 0.1 ppm) and all tests were carried out at room temperature (about 25℃) except the assigned tests at high (40℃) and low (-20℃)

temperatures (more detailed information about the abovementioned chemicals, reagents and materials can be seen in **Table S1**). Herein, the specific capacity (C_m, mAh g^{-1}), energy density (E_m, Wh kg^{-1}) and power density (P_m, kW kg^{-1}) of the NNO//KS6 Li-DIBs are calculated according to the **Equations S(1), S(2) and S(3)**.

$$C_m = It/3.6m \quad \text{S(1)}$$

$$E_m = C_m V \quad \text{S(2)}$$

$$P_m = 3.6E_m/t \quad \text{S(3)}$$

Where m refers to the masses of active electrode materials of both anode and cathode (g), which does not include the masses of the binder and acetylene black, and the electrolyte involved in the redox reactions is not considered either; V, I and t refer to the discharging voltage platforms (V), current (A) and discharging time (s), respectively.

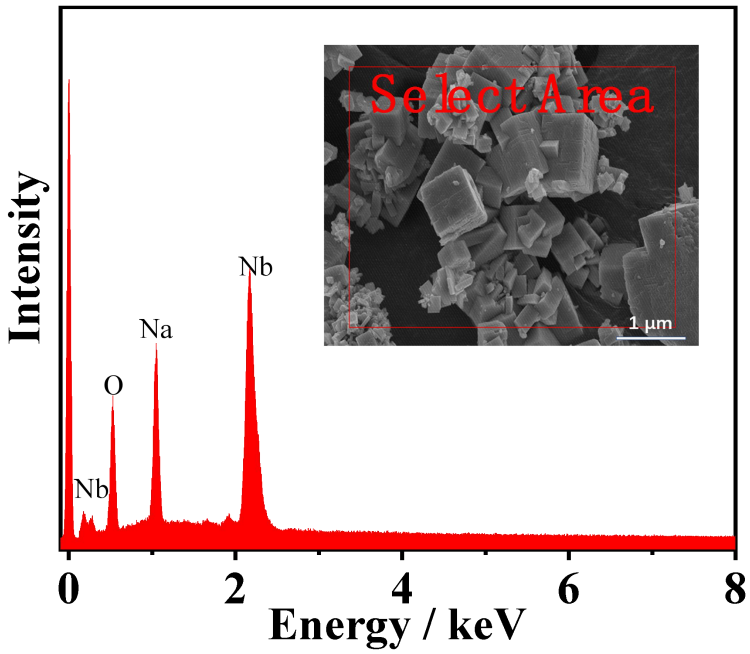

Fig. S1 EDS and select area of the NNO sample.

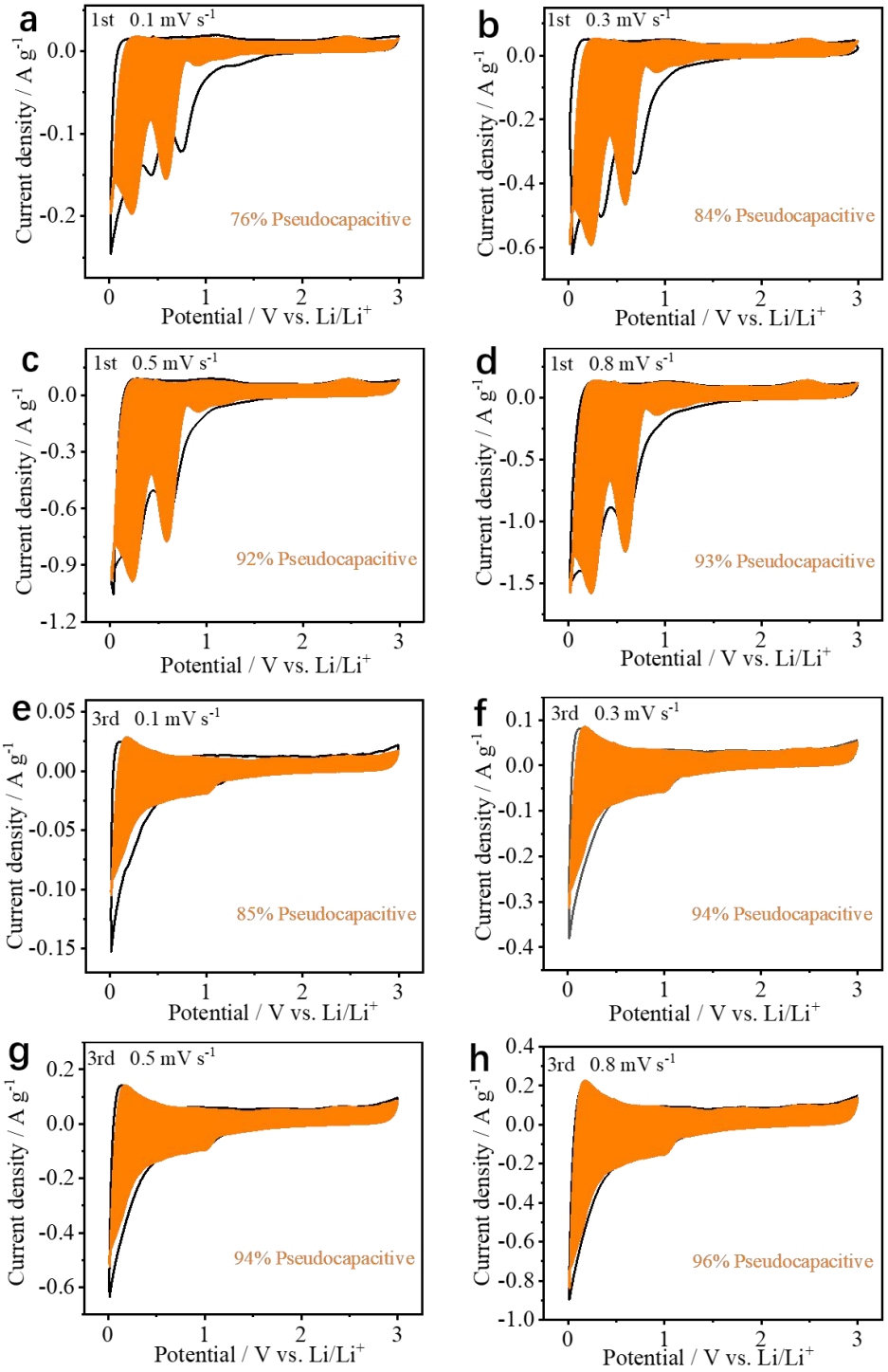

Fig. S2 The pseudocapacitive and diffusion-controlled contributions to charge storage in the NNO electrode (the shaded region is the identified pseudocapacitive contribution).

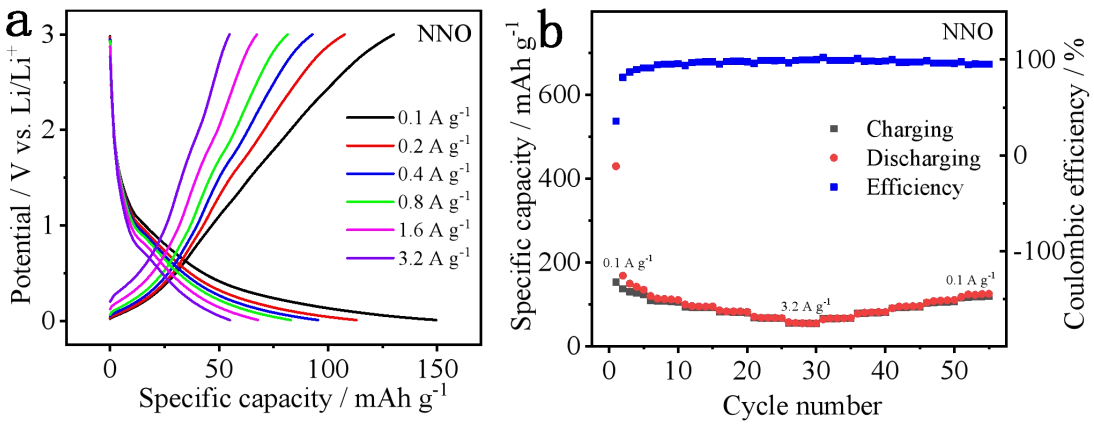

Fig. S3 GCD plots and rate behavior at 0.1-3.2 A g^{-1} of the NNO electrode.

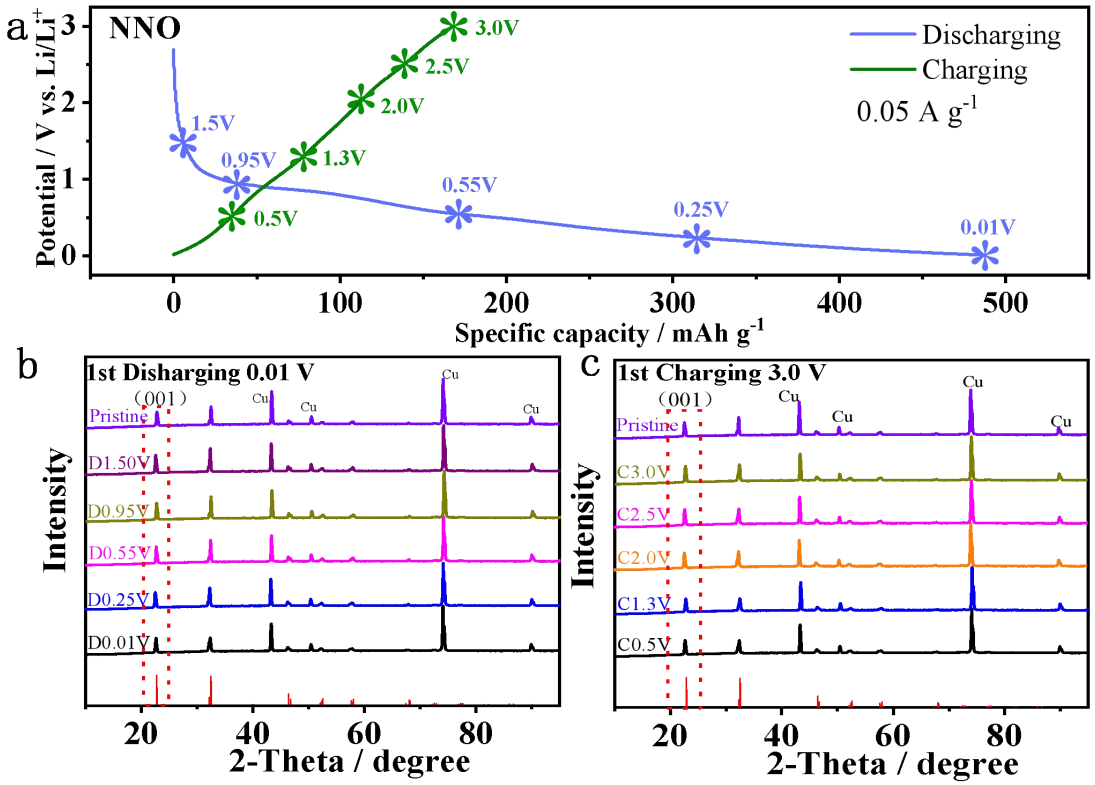

Fig. S4 The selected voltage states during the first cycle of GCD curves at 0.05 A g^{-1} (a), ex situ XRD patterns for the discharging (b) and charging (c) processes of the NNO electrode.

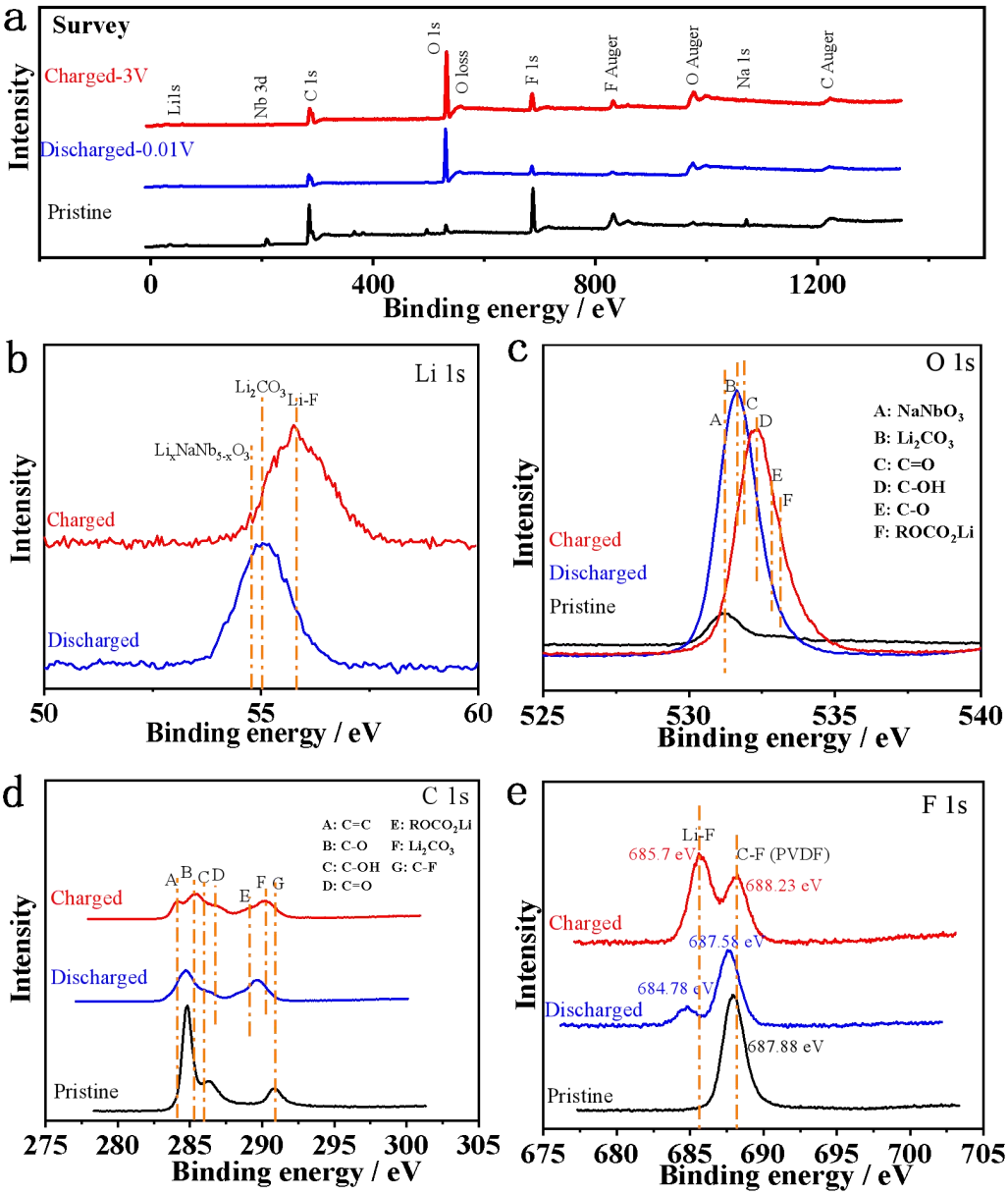

Fig. S5 Ex situ XPS for survey (a), Li 1s (b), O 1s (c), C 1s (d) and F 1s (e) in pristine and fully discharged/charged states of the NNO electrode.

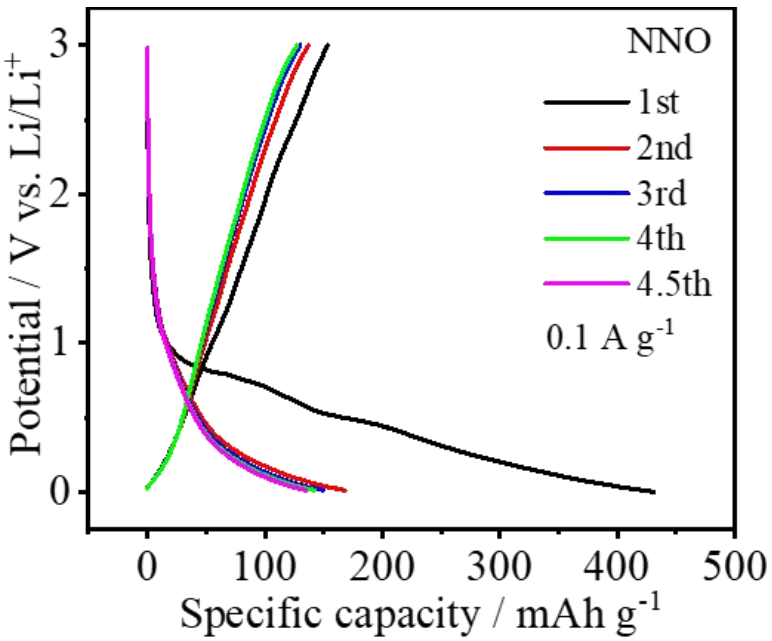

Fig. S6 The pre-charged (pre-lithiated) GCD plots at 0.1 A g^{-1} for 4.5 cycles of the NNO electrode.

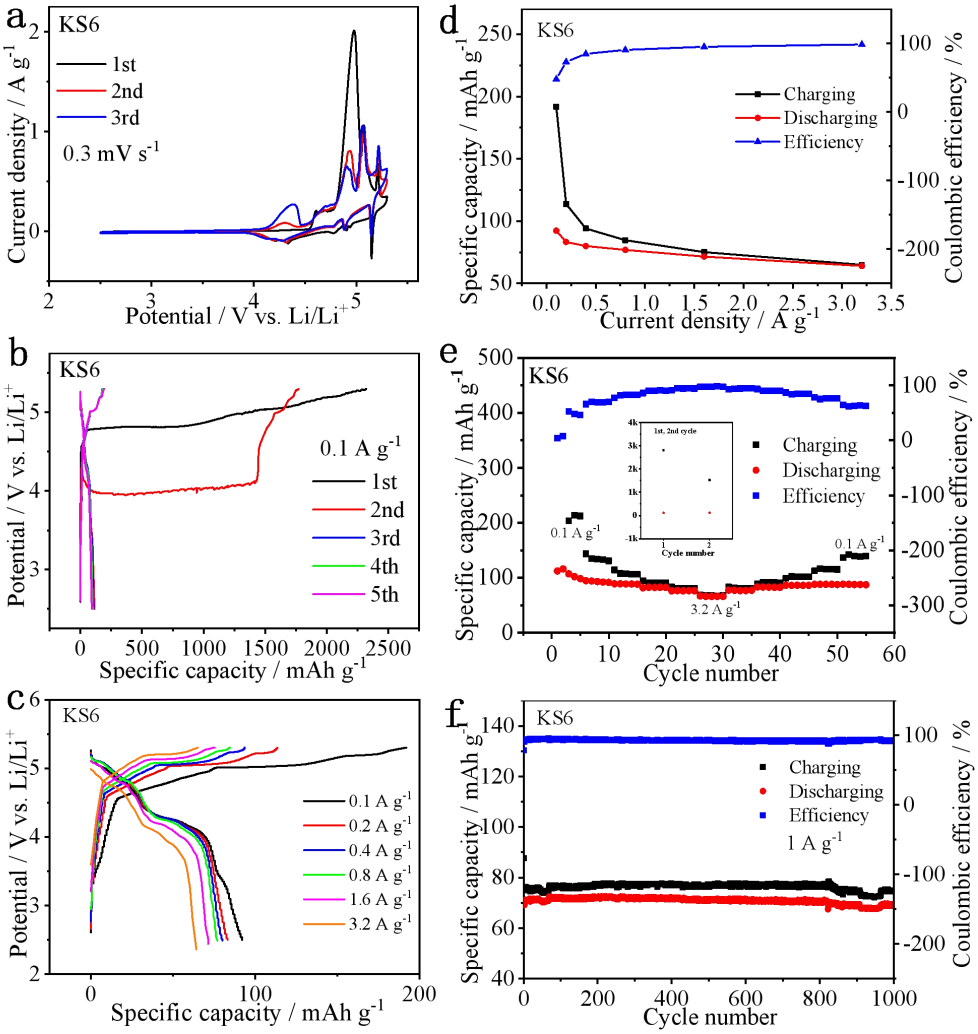

Fig. S7 Electrochemical performance of the KS6 electrode: CV plots for the first three cycles at 0.3 mV s^{-1} (a); GCD curves for the first five cycles at 0.1 A g^{-1} (b) and for the 5th cycle at 0.1-3.2 A g^{-1} (c); specific capacity, rate capability and coulombic efficiency at 0.1-3.2 A g^{-1} (d-e); cycling behavior at 1 A g^{-1} (f).

Graphite (KS6) was chosen as the cathode for the construction of the NNO//KS6 Li-DIBs. **Fig. S7**a-c show the CV plots and GCD curves, which show more than three pairs of redox peaks and charging/discharging plateaus in potential range of 2.5-5.3 V, suggesting the multi-steps co-insertions of PF_6^- anions and solvents in the graphite layers.[4] Note that the charging specific capacity of the KS6 electrode for the first two cycles is so large, which may be owing to the highly irreversible kinetics (i.e. the intercalation rate is far faster than the corresponding de-intercalation rate) at the low charging rates. The specific capacity, rate capability and cycling behavior are shown in **Fig. S7**d-f, showing that the KS6 electrode exhibits the specific capacity values of 92-64 mAh g^{-1} at 0.1-3.2 A g^{-1} and 83% retention for 1000 cycles at 1 A g^{-1} (**Table S2,** ESI). Such an excellent performance of KS6 can be a good cathode material used in Li-DIBs and will contribute to the advanced performance of the NNO//KS6 Li-DIBs.

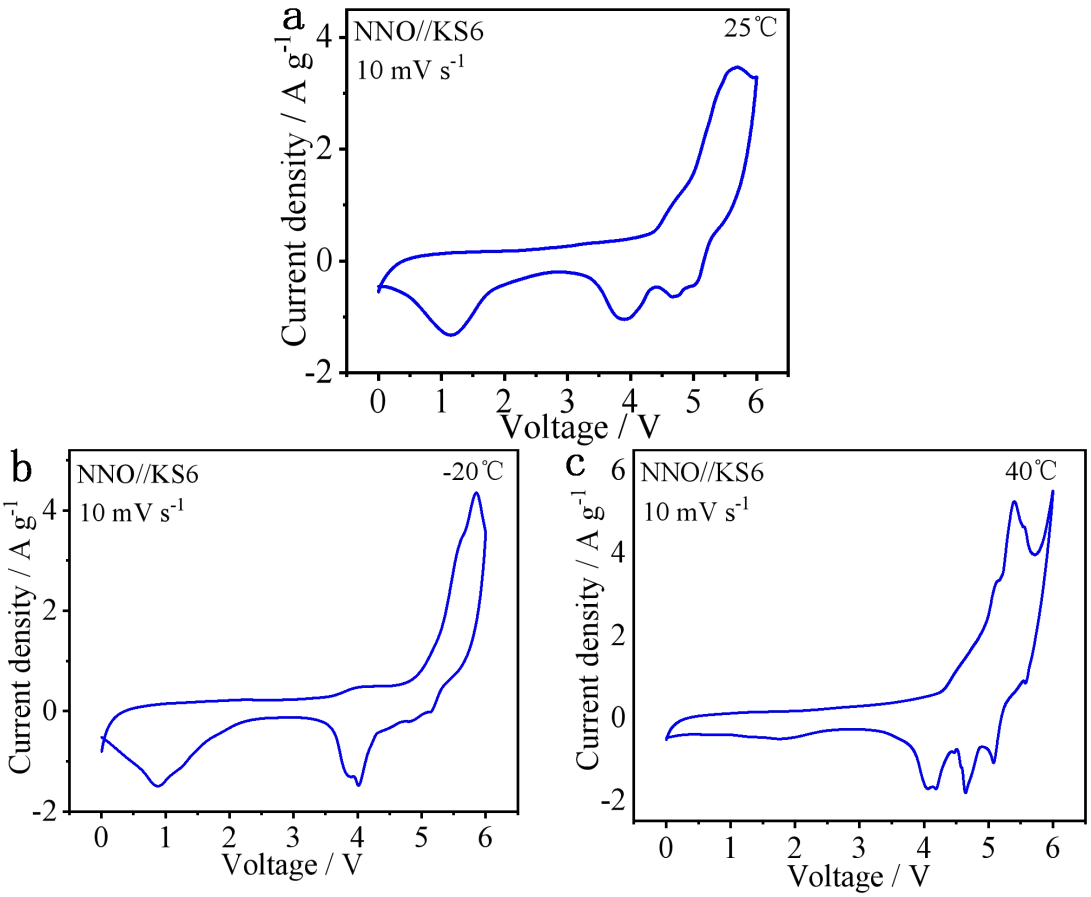

Fig. S8 The voltage windows of the NNO//KS6 Li-DIBs at room (25℃) (a), low (-20℃) (b) and high (40℃) temperatures (c).

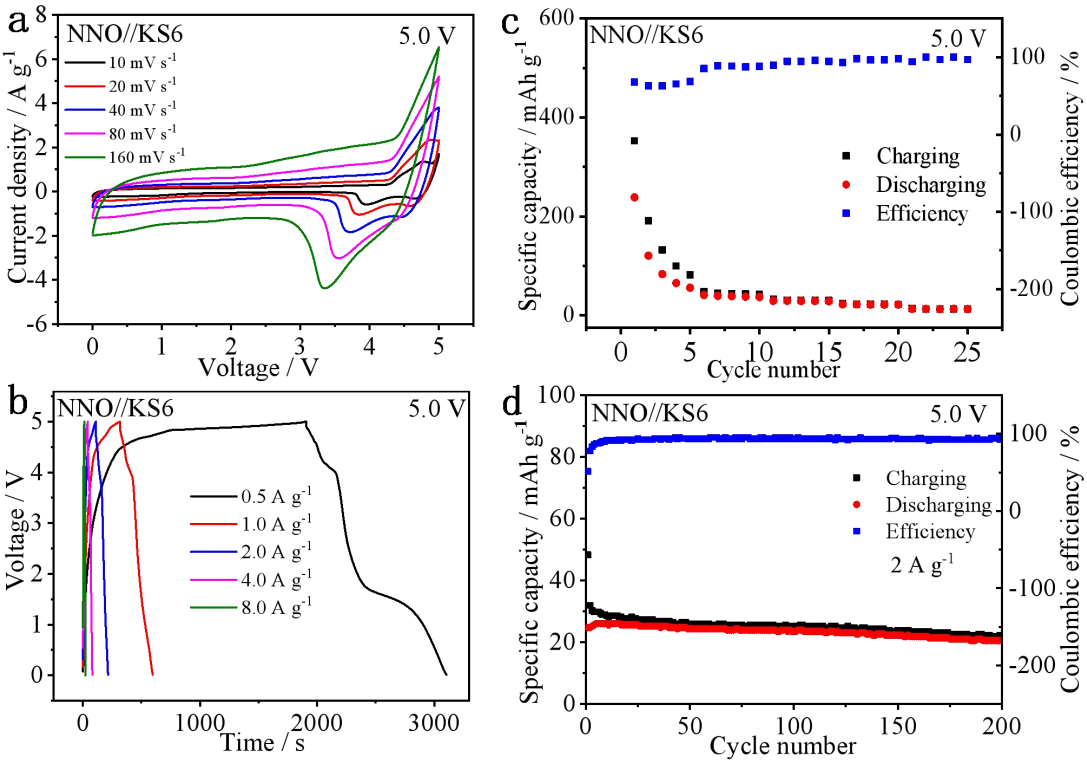

Fig. S9 The performance of the NNO//KS6 Li-DIBs under 0.01-5.0 V at room temperature (25℃) : CV plots at 10-160 mV s^{-1} (a), GCD curves at 0.5-8 A g^{-1} (b), rate capability at 0.5-8 A g^{-1} (c) and cycling behavior at 2 A g^{-1} (d).

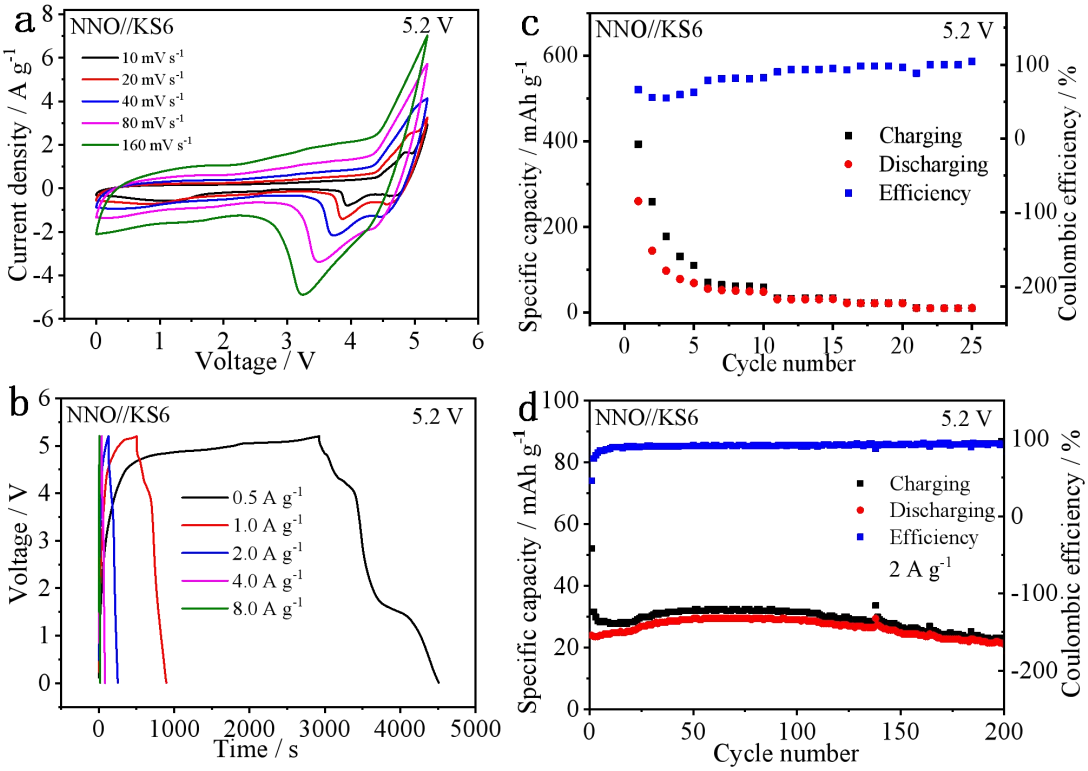

Fig. S10 The performance of the NNO//KS6 Li-DIBs under 0.01-5.2 V at room temperature (25℃) : CV plots at 10-160 mV s^{-1} (a), GCD curves at 0.5-8 A g^{-1} (b), rate capability at 0.5-8 A g^{-1} (c) and cycling behavior at 2 A g^{-1} (d).

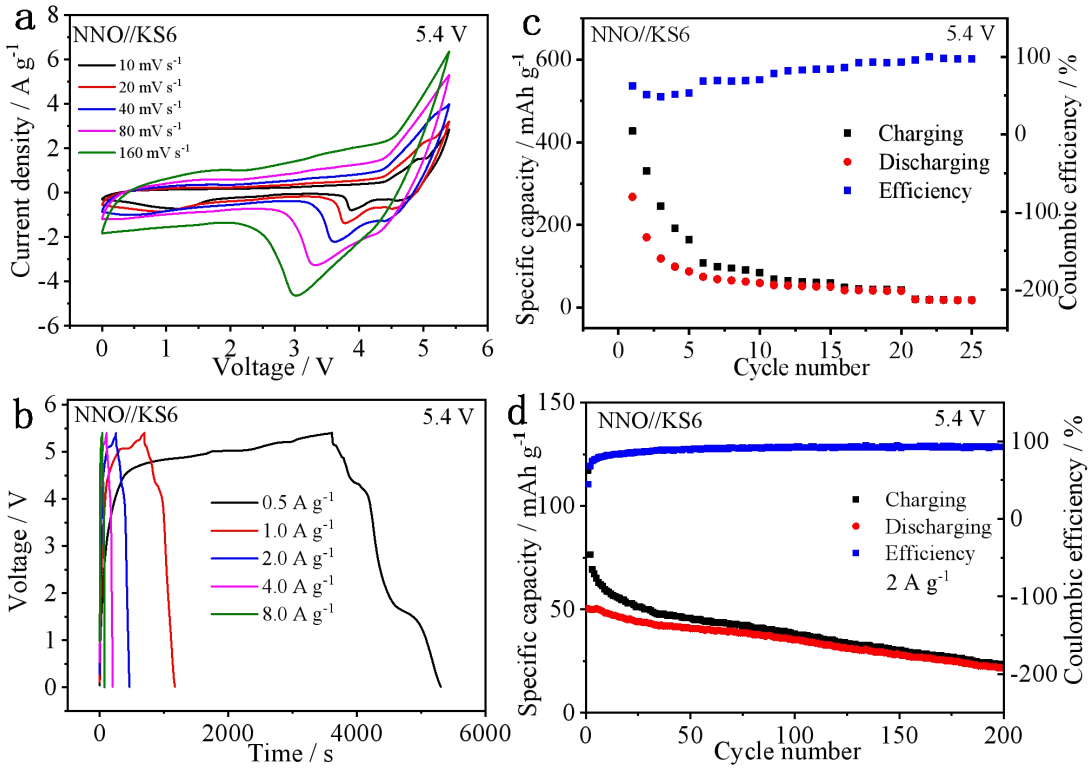

Fig. S11 The performance of the NNO//KS6 Li-DIBs under 0.01-5.4 V at room temperature (25℃) : CV plots at 10-160 mV s^{-1} (a), GCD curves at 0.5-8 A g^{-1} (b), rate capability at 0.5-8 A g^{-1} (c) and cycling behavior at 2 A g^{-1} (d).

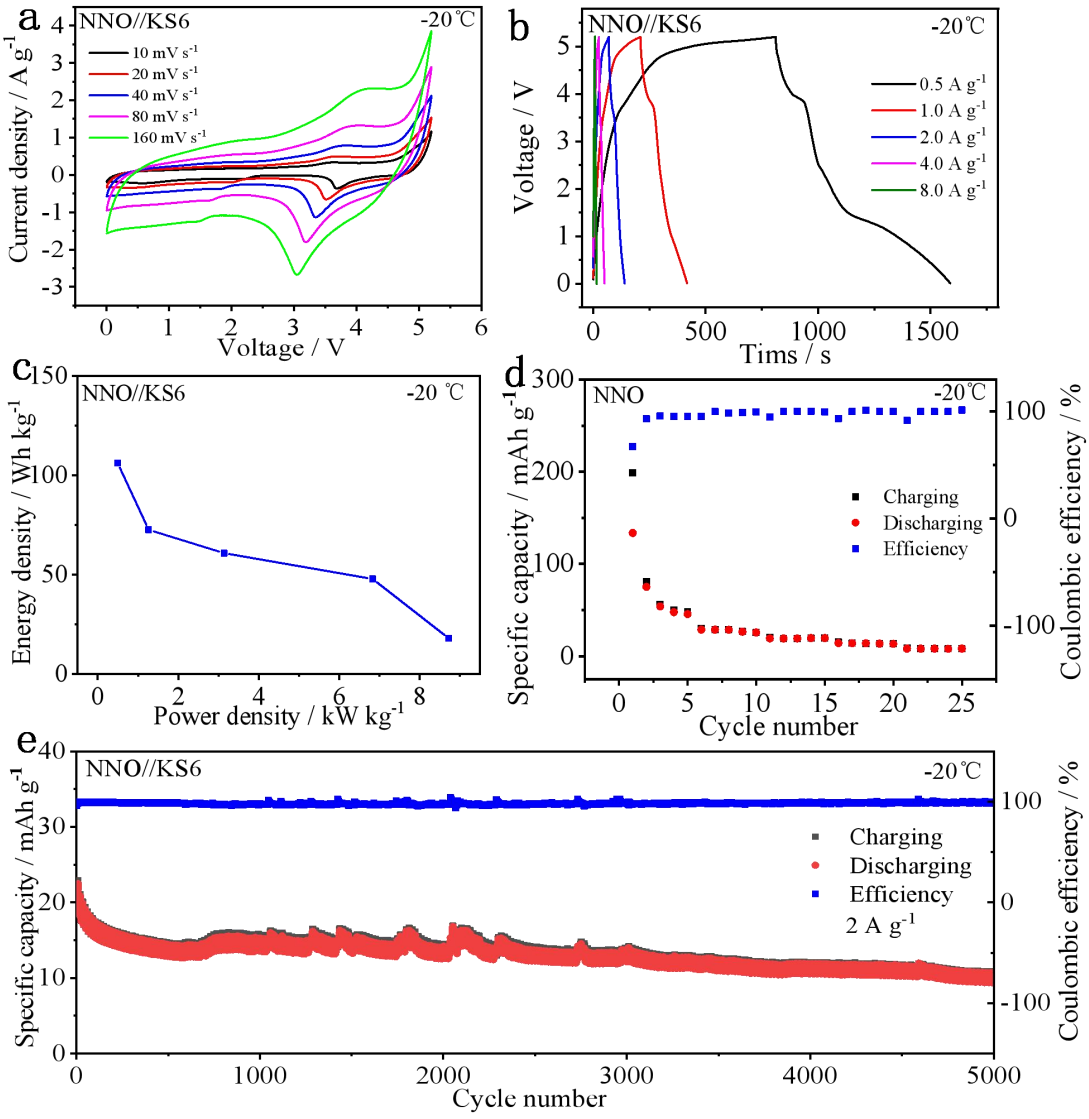

Fig. S12 The performance of the NNO//KS6 Li-DIBs under 0.01-5.2 V at low (-20℃) temperature: CV plots at 10-160 mV s^{-1} (a), GCD curves at 0.5-8 A g^{-1} (b), Ragone plots (c), rate capability at 0.5-8 A g^{-1} (d) and cycling behavior at 2 A g^{-1} (e).

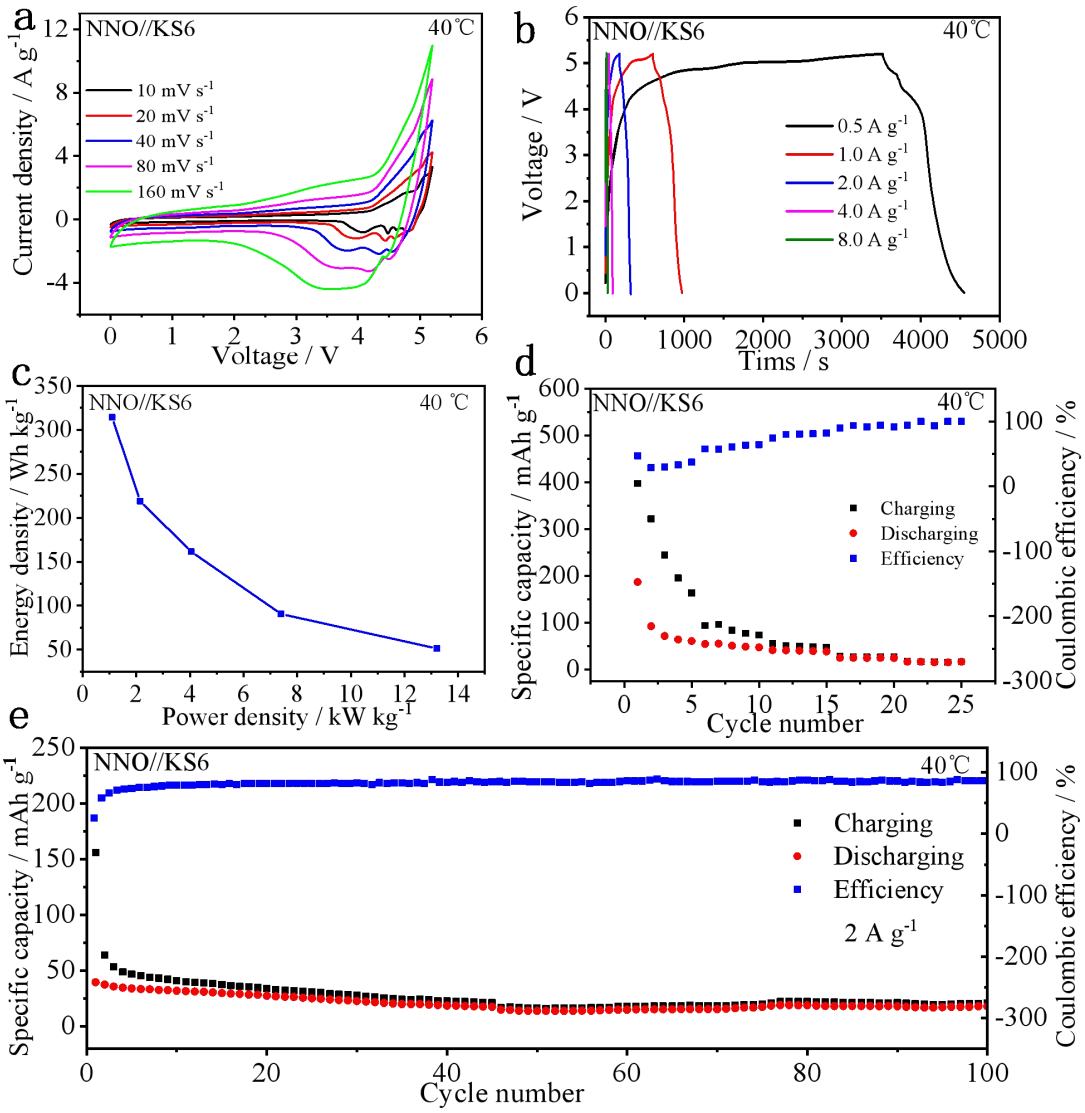

Fig. S13 The performance of the NNO//KS6 Li-DIBs under 0.01-5.2 V at high (40℃) temperature: CV plots at 10-160 mV s^{-1} (a), GCD curves at 0.5-8 A g^{-1} (b), Ragone plots (c), rate capability at 0.5-8 A g^{-1} (d) and cycling behavior at 2 A g^{-1} (e).

Table S1. Chemicals, reagents and materials used in the study.

Chemicals, reagents and materials	Type	Company	Characteristics
Nb_2O_5	AR	SinoPharm	purity≥99.99%
NaOH	AR	SinoPharm	purity≥96.0%
Graphite	KS6	TiMCAL	D90: 5.8-7.1 μm; Interlayer distance: 0.3354-0.3360 nm; SSA: 20 $m^2 g^{-1}$; Density-Scott: 0.07 g cm^{-3};
AB	Battery grade		/
Superconductive carbon black	Battery grade		/
NMP	AR	Kermel	purity≥99.0%
PVDF	Battery grade		/
Electrolytes	LBC-305-01	CAPCHEM	1 M $LiPF_6$/EC:EMC:DMC (1:1:1) /1% VC
Li plate	15.6*0.45 mm	China Energy	15.6*0.45 mm
Cu foil	200*0.015	GuangZhou JiaYuan	Total thickness: 15 μm; weight: 87 g m^{-2}
Carbon coated-Al foil	222*0.015	GuagZhou NaNuo	Total thickness: 17 μm; Strength: 192 Mpa
Glass microfiber filters	GF/D 2.7 μm; 1823-025	Whatman	Diameter: 25 mm; Thickness: 675 μm; weight: 121 g m^{-2}
Cell components	CR-2032	ShenZhen TianChenHe	/

Table S2. Specific capacity and cycling behavior of the NNO and KS6 electrodes.

Specific capacity (mAh g^{-1}) and cycling behavior of the NNO and KS6 electrodes								
Current density / (A g^{-1})	**0.1**	**0.2**	**0.4**	**0.8**	**1.6**	**3.2**	**Potential / V vs. Li/Li^+**	**Cycling behavior Retention% / 2 A g^{-1} (NNO) /1 A g^{-1} (KS6) / 1000 cycles**
NNO	130	107	92	82	98	55	0.01-3.0	185%
KS6	92	83	80	77	72	64	2.5-5.3	83%

Table S3. Performance summary of the NNO//KS6 Li-DIBs at room temperature (25^{o}C).

Cell system	Working voltage / V	Energy density / Wh kg^{-1}	Power density / kW kg^{-1}	Cycling behavior / retention%, repeated cycles, current density
NNO//KS6	0.01-5.0	181-95.7 77.2-55.6 -22.7	0.53-1.32 2.86-5.60 -8.70	95%/100/2 A g^{-1} 83%/200/2 A g^{-1}
	0.01-5.2	268-161 122-79.0 -26.1	0.70-1.60 3.97-7.30 -10.80	121%/100/2 A g^{-1} 104%/150/2 A g^{-1} 88%/200/2 A g^{-1}
	0.01-5.4	329-205 199-154 -60	0.74-1.65 3.80-8.18 -13.40	82%/50 /2 A g^{-1} 71%/100/2 A g^{-1} 56%/150/2 A g^{-1} 42%/200/2 A g^{-1}

Table S4. A comparison for the performance of the NNO//KS6 Li-DIBs in the study with some reported Li-DIBs.

Li-DIBs	Working voltage / V	Energy density / Wh kg^{-1}	Power density / kW kg^{-1}	Cycling behavior / retention%, repeated cycles, current density	Refs.
Graphite//Graphite	0.01-5.2	108	/	67%/50/0.05 A g^{-1}	5
Si-compound//Graphite	0-3	54	/	53%/100/0.1 A g^{-1}	6
Nb_2O_5//Graphite	1.5-3.5	52	/	84%/100/0.1 A g^{-1}	7
TiO_2//Graphite	1.5-3.7	36	/	88%/50/0.1 A g^{-1}	8
RGO//Graphite	0-4.0	70	1.33	74%/50/1.33 A g^{-1}	9
Li-DIBs based on some recently reported perovskite anodes					
$KNi_{0.1}Co_{0.9}F_3$//Graphite(918)	0.5-5.2	152	0.9	78%/200/2 A g^{-1}	10
$Na_{0.85}Ni_{0.45}Co_{0.55}F_{3.56}$//KS6	0.01-5.0	155.1	0.6	67%/200/2 A g^{-1}	11
NNO//KS6	**0.01-5.0**	**181-95.7 77.2-55.6 -22.7**	**0.53-1.32 2.86-5.60 -8.70**	**95%/100/2 A g^{-1} 83%/200/2 A g^{-1}**	**This work**
	0.01-5.2	**268-161 122-79.0 -26.1**	**0.70-1.60 3.97-7.30 -10.80**	**121%/100/2 A g^{-1} 88%/200/2 A g^{-1}**	
	0.01-5.4	**329-205 199-154 -60**	**0.74-1.65 3.80-8.18 -13.40**	**82%/50/2 A g^{-1} 71%/100/2 A g^{-1}**	

Table S5. Performance summary of the NNO//KS6 Li-DIBs under high (40^{o}C) and low (-20^{o}C) temperatures.

Cell system	T / ℃	Working voltage / V	Energy density / Wh kg^{-1}	Power density / kW kg^{-1}	Cycling behavior / retention%, repeated cycles, current density
NNO//KS6	40	0.01-5.2	314-219 162-90 -51	1.1-2.1 4.0-7.4 -13.2	60%/100/2 A g^{-1} 71%/2000/2 A g^{-1}
	-20	0.01-5.2	106-73 61-48 -18	0.5-1.3 3.1-6.8 -8.7	70%/3000/2 A g^{-1} 60%/4000/2 A g^{-1}

References

1 S. Y. Wu, W. Zhang and X. M. Chen, *J. Mater. Sci.: Mater. Electron.*, 2009, **21**, 450-455.

2 S. Y. Wu, X. Q. Liu and X. M. Chen, *Ceram. Int.*, 2010, **36**, 871-877.

3 H. Song and W. Ma, *Ceram. Int.*, 2011, **37**, 877-882.

4 J. A. Seel and J. R. Dahn, *J. Electrochem. Soc.*, 2000, **147**, 892-898.

5 J. A. Read, A. V. Cresce, M. H. Ervin and K. Xu, *Energy Environ. Sci.*, 2014, **7**, 617-620.

6 H. Nakano, Y. Sugiyama, T. Morishita, M. J. S. Spencer, I. K. Snook, Y. Kumai and H. Okamoto, *J. Mate. Chem. A*, 2014, **2**, 7588-7592.

7 G. Park, N. Gunawardhana, C. Lee, S.-M. Lee, Y.-S. Lee and M. Yoshio, *J. Power Sources*, 2013, **236**, 145-150.

8 A. K. Thapa, G. Park, H. Nakamura, T. Ishihara, N. Moriyama, T. Kawamura, H. Y. Wang and M. Yoshio, *Electrochim. Acta*, 2010, **55**, 7305-7309.

9 X. Y. Shi, W. Zhang, J. F. Wang, W. T. Zheng, K. K. Huang, H. B. Zhang, S. H. Feng, H. Chen, *Adv. Energy Mater.,* 2016, ***6***, 1601378.

10 Q. L. Xu, R. Ding, W. Shi, D. F. Ying, Y. F. Huang, T. Yan, P. Gao, X. J. Sun and E. H. Liu, *J. Mater. Chem. A*, 2019, **7**, 8315-8326.

11 W. Shi, R. Ding, Q. L. Xu, T. Yan, Y. X. Huang, C. N. Tan, X. J. Sun, P. Gao and E. H. Liu, *Chem. Commun.*, 2019, **55**, 6739-6742.